Modeling optical properties of human skin using Mie theory for particles with different size distributions and refractive indices

A. Bhandari,[1,*] **B. Hamre,**[1] **Ø. Frette,**[1] **K. Stamnes,**[2] **and J. J. Stamnes**[1]

[1]*Department of Physics and Technology, University of Bergen, Allegaten 55, 5007 Bergen, Norway*
[2]*Department of Physics and Engineering Physics, Stevens Institute of Technology, Hoboken, NJ, USA*
[*]*Anak.Bhandari@gfi.uib.no*

Abstract: We used size distributions of volume equivalent spherical particles with complex refractive index to model the inherent optical properties (IOPs) in four different layers of human skin at ten different wavelengths in the visible and near-infrared spectral bands. For each layer, we first computed the size-averaged absorption coefficient, scattering coefficient, and asymmetry factor for the collection of particles in a host medium using Mie theory and compared these IOPs in each layer with those obtained from a bio-optical model (BOM). This procedure was repeated, using an optimization scheme, until satisfactory agreement was obtained between the IOPs obtained from the particle size distribution and those given by the BOM. The size distribution as well as the complex refractive index of the particles, obtained from this modeling exercise, can be used to compute the phase matrix, which is an essential input to model polarized light transport in human skin tissue.

OCIS codes: (000.1430) Biology and medicine; (170.3660) Light propagation in tissues; (290.5850) Scattering, particles.

References and links

1. P. A. Payne, "Measurement of properties and function of skin," Clin. Phys. Physiol. Meas. **12**, 105-129 (1991).
2. M. Gillison, *A History of the Body Tissues* (Williams and Wilkins Co., Baltimore, Maryland, 1962).
3. B. L. Diffey, "A Mathematical model for ultraviolet optics in skin," Phys. Med. Biol. **28**, 647-657 (1983).
4. K. P. Nielsen, L. Zhao, P. Juzenas, J. J. Stamnes, K. Stamnes and J. Moan, "Reflectance spectra of pigmented and non-pigmented skin in the UV spectral region," Photochem. Photobiol. **80**, 450-455 (2004).
5. A. R. Young, "Chromophores in Human Skin," Phys. Med. Biol. **42**, 789-802 (1997).
6. D. J. Faber, M. C. G. Aalders, E. G. Mik, B. A. Hooper, M. J. C. van Gemert, and T. G. van Leeuwen, "Oxygen saturation-dependent absorption and scattering of blood," Phys. Rev. Lett. **93**, 1-4 (2004).
7. J. Sandby-Møller, T. Paulsen, and H. C. Wulf, "Epidermal thickness at different body sites: relationship to age, gender, pigmentation, blood content, skin type and smoking," Acta Derm. Venereol. **83**, 410-413 (2003).
8. A. N. Bashkatov, E. A. Genina, V. I. Kochubey, and V. V. Tuchin, "Optical properties of human skin, subcutaneous and mucous tissues in the wavelength range from 400 to 2000 nm," J. Phys. D: Appl. Phys. **38**, 2543-2555 (2005).
9. B. Farina, C. Bartoli, A. Bono, A. Colombo, M. Lualdi, G. Tragni, and R. Marchesini, "Multispectral imaging approach in the diagnosis of cutaneous melanoma: potentiality and limits," Phys. Med. Biol. **45**, 1243-1254 (2000).
10. M. Moncrieff, S. Cotton, E. Claridge, and P. Hall, "Spectrophotometric intracutaneous analysis - a new technique for imaging pigmented skin lesions," Br. J. Dermatol. **146**, 448-457 (2002).

#146310 - $15.00 USD Received 28 Apr 2011; revised 22 Jun 2011; accepted 23 Jun 2011; published 14 Jul 2011

11. M. J. C. Van Gemert, S. L. Jacques, H. J. C. M. Sterenborg, and W. M. Star, "Skin Optics," IEEE Trans. Biomed. Eng. **36**, 1146-1154 (1989).
12. S. L. Jacques, "Role of tissue optics and pulse duration on tissue effects during high-power laser irradiation," Appl. Opt. **32**, 2447-2454 (1993).
13. R. R. Anderson and J. A. Parrish, "The optics of human skin," J. Invest. Dermat. **77**, 13-19 (1981).
14. A. Yodh and B. Chance, "Spectroscopy and imaging with diffusing light," Phys. Today **48**, 34-40 (1995).
15. J. Mobley and T. V. Dinh, "Optical properties of tissue," *in Biomedical Photonics Handbook*, T. V. Dinh, ed.(CRC press, 2003), pp. 12-36.
16. J. R Mourant, J. P. Freyer, A. H. Hielscher, A. A. Eick, D. Shen, and T. M. Johnson, "Mechanisms of light scattering from biological cells relevant to non-invasive optical-tissue diagnostics," Appl. Opt. **37**, 3586-3593 (1998).
17. S. L. Jacques, "Optical assessment of tissue heterogeneity in biomaterial and implants," Proc. SPIE **3914**, 576-580 (2000), doi:10.1117/12.388080.
18. R. Drezek, A. Dunn, and R. Richards-Kortum, "Light scattering from cells: finite-difference, time-domain simulations and goniometric measurements," Appl. Opt. **38**, 3651-3661 (1999).
19. K. P. Nielsen, L. Zhao, J. J. Stamnes, K. Stamnes, and J. Moan, "Importance of the depth distribution of melanin in skin for DNA protection and other photobiological processes," J. Photochem. Photobiol. **82**, 194-198 (2006).
20. I. S. Saidi, S. L. Jacques, and F. K. Tittel, "Mie and Rayleigh modelling of visible light scattering in neonatal skin," Appl. Opt. **34**, 7410-7418 (1995).
21. G. J. Tearney, M. E. Brezinski, J. F. Southern, B. E. Bouma, M. R. Hee, and J. G. Fujimoto, "Determination of the refractive index of highly scattering human tissue by optical coherence tomography," Opt. Lett. **20**, 2258 -2260 (1995).
22. H. Ding, J. Q. Lu, W. A. Wooden, P. J. Kragel, and X.-H. Hu, "Refractive indices of human skin tissues at eight wavelengths and estimated dispersion relations between 300 and 1600 nm," Phys. Med. Biol. **51**, 1479-1489, (2006).
23. J. R. Fristvad, N. J. Christensen, and H. W. Jensen, "Computing the scattering properties of participating media using Lorenz-Mie theory," ACM Trans. Graph. **26**, 1-10 (2007).
24. Q. Fu and W. Sung, "Mie theory for light scattering by a spherical particle in an absorbing medium," Appl. Opt. **40**, 1354-1361 (2001).
25. P. C. Waterman, "Symmetry, unitarity, and geometry in electromagnetic scattering," Phys. Rev. D **3**, 825-839 (1971).
26. M. I. Mishchenko, L. D. Travis, and D. W. Mackowski, "T-matrix computations of light scattering by nonspherical particles: A Review," J. Quant. Spectr. Radiat. Transfer **55**, 535-575 (1996).
27. A. M. K. Nilsson, P. Alshom, A. Karlson, and S. A. Andersson-Engels, "T-matrix computations of light scattering by red blood cells," Appl. Opt. **37**, 2735-2747 (1998).
28. D. Petrov, E. Synelnyk, Y. Shkuratov, and G. Videen, "The T-matrix technique for calculations of scattering properties of ensembles of randomly oriented particles with different size," J. Quant. Spectr. Radiat. Transfer **102**, 85-110 (2006).
29. A. J. Cox, A. J. Deweerd, and J. Linden, "An experiment to measure Mie and Rayleigh total scattering cross sections," Am. J. Phys. **70**, 620-625 (2002).
30. S. L. Jacques, "Optical assessment of cutaneous blood volume depends on the vessel size distribution: a computer simulation study," J. Biophoton. **3**, 75-81 (2010). DOI 10.1002/jbio.200900085.
31. C. F. Bohren and D. R. Huffman, *Absorption and Scattering of Light by Small Particles* (A Wiley-VCH, GmbH & Co. Weinheim, 2004), pp. 82-129.
32. H. C. Van de Hulst, *Light Scattering by Small Particles* (Dover Publications Inc., New York, 1957), pp. 103-130.
33. W. J. Wiscombe, "Improved Mie scattering algorithms," Apl. Opt. **19**, 1505-1509 (1980).
34. W. A. de Rooij and C. C. A. H. Van der Stap, "Expansion of Mie scattering matrices in generalized spherical functions," Astron. Astrophys. **131**, 237-248 (1984).
35. M. I. Mishchenko, "The electromagnetic optical theorem revisited," J. Quant. Spectr. Radiat. Transfer **101**, 404-410 (2006).
36. G. E. Thomas and K. Stamnes, *Radiative Transfer in the Atmosphere and Ocean* (Cambridge University Press, 2002), pp. 74-79.
37. M. Jermy, "New model for light propagation in highly inhomogeneous polydisperse turbid media with applications in spray diagnostics," Opt. Express **13**, 1981-1995 (2005).
38. E. Limpert, W. A. Stahel, and M. Abbt, "Log-normal distributions across the science: keys and clues," BioScience **51**, 341-351 (2001).
39. B. Hamre, J. Winther, S. Gerland, J. J. Stamnes, and K. Stamnes, "Modelled and measured optical transmittance of snow-covered first-year sea ice in Kongfjorden, Svalbard," J. Geophys. Res. **109**, 1-14 (2004).
40. H. J. van Staveren, C. J. M. Moes, J. van Marie, S. A. Prahl, and M. J. C. van Gemert, "Light scattering in intralipid-10% in the wavelength range of 400-1100 nm," Appl. Opt. **30**, 4507-4514, (1991).
41. K. P. Nielsen, L. Zhao, G. A. Ryzhikov, M. S. Biryulina, E. R. Sommersten, J. J. Stamnes, K. Stamnes, and J. Moan, "Retrieval of the physiological state of human skin from UV-VIS reflectance spectra - A feasibility study,"

#146310 - $15.00 USD Received 28 Apr 2011; revised 22 Jun 2011; accepted 23 Jun 2011; published 14 Jul 2011

J. Photochem. Photobiol. B **93**, 23-31 (2008).
42. M. J. C. van Gemert, A. J. Welch, W. M. Star, M. Motamedi, and W.-F. Cheong, "Tissue Optics for a slab geometry in the diffusion approximation," Laser Med. Sci. **2**, 295-302 (1987). DOI: 10.1007/BF02594174
43. D. L. Swanson, S. D. Laman, M. Biryulina, K. P. Nielsen, G. Ryzhikov, J. J. Stamnes, B. Hamre, L. Zhao, F. S. Castellana, and K. Stamnes, "Optical transfer diagnosis of pigmented lesions: a pilot study," Skin Res. Technol. **15**, 330–337 (2009). doi: 10.1111/j.1600-0846.2009.00367.x
44. K. Zhang, W. Li, H. Eide, and K. Stamnes, "A bio-optical model suitable for use in forward and inverse coupled atmosphere-ocean radiative transfer models," J. Quant. Spectr. Radiat. Transfer **103**, 411-4233 (2007).
45. A. N. Bashkatov, E. A. Genina, V. I. Kochubey, and V. V. Tuchin, "Estimation of wavelength dependence of refractive index of collagen fibers of scleral tissue," Proc. SPIE **4162**, 265-267 (2000).
46. D. L. Swanson, S. D. Laman, M. Biryulina, K. P. Nielsen, G. Ryzhikov, J. J. Stamnes, B. Hamre, L. Zhao, E. Sommersten, F. S. Castellana, and K. Stamnes, "Optical transfer diagnosis of pigmented lesions," Dermatol. Surg. **36**, 1-8 (2010). DOI: 10.1111/j.1524-4725.2010.01808.x
47. R. L. P. Van Veen, H. J. C. M. Sterenborg, A. Pifferi, A. Torricelli, and R. Cubeddu, "Determination of VIS-NIR absorption coefficients of mammalian fat with time- and spatially resolved diffuse reflectance and transmission spectroscopy," OSA Annual BIOMED Topical Meeting (2004).
48. D. J. Segelstein, "The complex refractive index of water," M.Sc. thesis, University of Missouri, Kansas City (1981).
49. S. Prahl, "Tabulated Molar Extinction Coefficient for Hemoglobin in Water," http://omlc.ogi.edu/spectra/hemoglobin/takatani.html.
50. R. M. Lewis, V. Torczon, and M. W. Trosset, "Direct search methods: then and now," J. Compt. Appl. Math. **124**, 191-207, (2000).
51. J. C. Lagarias, J. A. Reeds, M. H. Wright, and P. E. Wright, "Convergence properties of the Nelder-Mead simplex method in low dimensions," SIAM J: Optimization **9**, 112-147 (1998).
52. J. A. Nelder and R. Mead, "A simplex method for function minimization," Comp. Jour. **7**, 308-313 (1965).
53. http://www.baltermedical.com/.
54. C. Mätzler, "MATLAB functions for Mie scattering and absorption," Inst. Appl. Phys., University of Bern (2002), http://arrc.ou.edu/∼rockee/NRA_2007_website/Mie-scattering-Matlab.pdf.
55. K. Hestenes, K. P. Nielsen, L. Zhao, J. J. Stamnes, and K. Stamnes, "Monte Carlo and discrete-ordinate simulations of spectral radiances in a coupled air-tissue system," Appl. Opt. **46**, 2333-2350 (2007).
56. C. Magnain, M. Elias, and J. Frigerio, "Skin color modelling using the radiative transfer equation solved by the auxiliary function method," J. Opt. Soc. Am. A **24**, 2196-2203 (2007).
57. A. N. Bashkatov, E. A. Genina, and V. V. Tuchin, "Optical properties of skin, subcutaneous and mucous tissues: A review," J. Innov. Opt. Health Sci. Appl. Phys. **4**, 9-38 (2011).
58. V. V. Tuchin, I. L. Maksinova, D. A. Zimnyakov, I. L. Kon, A. H. Mavlutov, and A. A. Mishin, "Light propagation in tissues with controlled optical properties," J. Biomed. Opt. **2**, 401-417 (1997).
59. J. C. Lai, Y. Y. Zhang, Z. Li, H. Jiang, and A. He, "Complex refractive index measurement of biological tissues by attenuated total ellipsometry," Appl. Opt. **49**, 3235-3237 (2010).
60. S. Chandrasekhar, *Radiative Transfer* (Dover Publication, Inc. N.Y., 1960).
61. E. J. Dennis, G. J. Dolmans, R. K. Jain, and D. Fukumura, "Photodynamic therapy for cancer," Nature Reviews Cancer **3**, 380-387 (2003).

1. Introduction

Skin is the largest organ of the human body and is important for protection, sensation, and thermoregulation. Human skin consists of three main layers [1], the *epidermis*, the *dermis*, and the *sub-cutis*, each being a heterogeneous medium for transport of light. The epidermis ($\approx$100 μm), which is thinner than the dermis ($\approx$1 mm) and the sub-cutis ($\approx$3 mm), may be further divided into sub-layers [2], namely the *stratum corneum*, the *stratum lucidum*, the *stratum granulosum*, the *stratum spinosum*, and the *stratum germinativum*. The stratum corneum which is 10–20 μm thick, is the outermost layer of the epidermis, and is composed of non-living *corneocyte* cells glued together with *keratin* to form a membrane-like structure.

Human skin shows characteristic photo-biological responses to ultraviolet (UV), visible (VIS), and near-infrared (NIR) radiation. In the UV spectral range, such processes include erythema, carcinogenesis, and melanogenesis [3]. Keratin, melanin, and DNA particles in the epidermis absorb UV radiation [4], and act as barriers against UV penetration into the underlying skin layers. The oxygenated and deoxygenetated blood particles in the dermis strongly absorb VIS radiation [5, 6], and the water contained in skin tissues absorbs NIR radiation.

#146310 - $15.00 USD Received 28 Apr 2011; revised 22 Jun 2011; accepted 23 Jun 2011; published 14 Jul 2011

These characteristic photo-biological responses of human skin tissue strongly depend on skin type, age, and body site of individuals, and also on gender [7, 8]. Changes in the color of the skin surface due to such photo-biological responses can provide diagnostic information useful for dermatologists to assess skin tissue abnormalities. Multi-spectral photographs of pigmented skin lesions have been intensively investigated to diagnose early stages of skin cancer [9, 10] *in vivo*.

When a skin surface is illuminated, a fraction of the incident radiation is specularly reflected from it, with reflectance given by the Fresnel equation, due to the change in the refractive index across the air-skin interface. The penetration of radiative energy into the interior of the skin is strongly regulated by the amount of melanin and keratin in the epidermis, blood and collagen in the dermis, and fat and connective tissues in the sub-cutis. The structural units, such as cell walls, cell membranes, cell organelles, nuclei, mitochondria, and other organic and inorganic substances in each layer, are embedded into the base fluid of the bulk tissue. These structural particles in tissues are responsible for the absorption and scattering of the radiation depending on their complex refractive indices, shapes, and concentration. The spatial alignment of structural particles in tissues such as collagen in the dermis shows birefringence effects, which affect the polarization of light. However, pursuing such optical properties is beyond the scope of this work.

As a function of wavelength λ, the absorption coefficient $\mu_a(\lambda)$ [mm^{-1}] of a particle embedded in a base fluid or host medium can be expressed by

$$\mu_a(\lambda) \simeq f_a\,\mu_{a,p}(\lambda) + (1 - f_a)\,\mu_{a,h}(\lambda) \tag{1}$$

where f_a is the volume fraction occupied by the absorbing particle, and where $\mu_{a,p}(\lambda)$ and $\mu_{a,h}(\lambda)$ are the absorption coefficients of the particle and host medium, respectively. If the absorption by each particle is assumed to be independent of the absorption by all other particles, the net absorption coefficient for a collection of N particles becomes N times $\mu_{a,p}(\lambda)$.

The attenuation of the incident radiation due to absorption alone can be explained by Beer-Lambert's exponential law [11, 12], which in the case of negligible scattering has been employed in *in vitro* investigations of tissues of e.g. arteries, liver, and kidney. However, the attenuation of VIS and NIR radiation in human skin tissue due to absorption is much less than that due to scattering [11, 13], and the radiation emerging from the skin surface is diffuse due to random multiple scattering events. Diffuse scattering of VIS and NIR radiation from biological tissue has been intensively investigated for a long time to develop non-invasive diagnostic techniques, particularly in the field of medicine [14]. Such diagnostic techniques rely on the wavelength-dependent extinction in different tissues. The radiation that penetrates deepest into skin tissue is within the combined VIS and NIR spectral range, which is known as the *therapeutic window* [15].

The spatial fluctuation of the refractive index as well as the structural arrangement of cellular particles make skin tissues optically heterogeneous, and light scattering occurs due to mismatch of the refractive indices at boundaries between particles and the host medium. A variety of reports exist on the size distribution of particles in biological tissues. According to Mourant et al. [16], the volume of scattering particles in mammalian cells is equivalent to that of a collection of spheres with diameters in the order of 0.4 to 20 μm, while Jacques [17] reported that scattering in biological tissue is due to particles in the size range of 0.1 to 10 μm. According to Drezek et al. [18], sizes of cellular particles such as mitochondria ranges from 0.05 to 1.5 μm. Similarly, the shape of scattering particles varies. Keratin cells in the stratum corneum are flat, and melanosome particles in the lower epidermis (stratum germanitivum) are fairly round with a diameter of about 1 μm [3]. But melanosome particles become fragmented [19] as they move upwards from the lower epidermis, and end up as small melanin dust particles in the upper epidermis. Normal blood cells are disc shaped, but the shape becomes deformed when they

#146310 - $15.00 USD Received 28 Apr 2011; revised 22 Jun 2011; accepted 23 Jun 2011; published 14 Jul 2011

flow in the blood vessels. The collagen aggregates, which are the most abundant protein in the dermis layer, are of various sizes, shapes, and orientations. Saidi et al. [20] measured the size of collagen fibers and fibrils and found them to be about 1-8 μm and 100 nm, respectively, in skin samples of newborn infants.

The variation in the refractive index of tissue constituents published in the literature was summarized by Drezek et al. [18], according to which the real part of the refractive index varies from 1.36 for extracellular fluids to 1.7 for melanosome particles. Tearney et al. [21] found the real part of the refractive index of human dermis and adipose tissues to be equal to 1.400 ± 0.007 and 1.467 ± 0.008, respectively.

The refractive indices referred to above include only the real part, implying that no information about absorption is given. However, melanosome and hemoglobin particles both scatter and absorb light. The complex refractive indices for *Caucasian* and *African American* human skin epidermis and dermis *in vitro* were measured by Ding et al. [22] at several wavelengths in the 300 to 1600 nm spectral range. Their results showed that the real part of the complex refractive index decreases with increasing wavelength both in the epidermis and dermis. Moreover, the values of the real part of the refractive index measured in the epidermis were higher than those in the dermis. The scattering occurs because of the spatial inhomogeneity of the refractive index of the particles relative to that of the host medium. When the host medium is non-absorbing, light absorption is only due to embedded particles. However, in an absorbing host medium, both incident and scattered light will be absorbed also by the host medium depending on the size of the imaginary part of its refractive index. At longer wavelengths, the skin dermis may be absorbing, in which case a description based on scattering by spherical particles embedded in a non-absorbing medium (Mie theory) may need to be modified [23]. Investigations have shown that an absorbing medium affects the scattering phase function [24] of larger sized particles. We disregarded such effects, assuming the host medium to be non-absorbing with a constant real-valued refractive index in each layer, but assuming all embedded particles in the host medium to have a complex refractive index.

Light scattering by non-spherical, smooth, homogeneous particles can be described by the T-matrix method [25–28] as long as its shape does not deviate too much from that of a sphere and the size is not too large. Since particle shapes in skin tissues are not well known, we assumed for simplicity a size distribution of spherical particles in each of the skin layers. Moreover, we assumed the spherical particles in each layer to be embedded in a non-absorbing host medium of constant refractive index. Then light scattering can be described by a combination of Mie scattering for particles with sizes comparable to the wavelength of the incident light and Rayleigh scattering for particles that are small compared to the wavelength of the incident light. The scattering coefficient $\mu_s(\lambda)$ [mm^{-1}] due to combined contributions from both Mie and Rayleigh scattering can then be expressed by

$$\mu_s(\lambda) \simeq f_s\lambda^{-b} + (1-f_s)\lambda^{-4} \tag{2}$$

where f_s is the fraction of scattering due to large particles contributing to Mie scattering, $(1-f_s)$ is the fraction of scattering due to small particles contributing to Rayleigh scattering, and b indicates the wavelength dependence of Mie scattering.

The size of a spherical particle of radius r may be expressed in terms of a dimensionless *size* parameter $x = 2\pi r/\lambda$, where λ is the wavelength of light in the medium. Particles with $x \ll 1$, pertain to Rayleigh scattering [29] with wavelength dependence given by λ^{-4}, and with the angular distribution of the scattering being equally probable in the forward and the backward direction. Rayleigh scattering is independent of the particle shape [31] as long as the condition $x \ll 1$ is fulfilled.

#146310 - $15.00 USD Received 28 Apr 2011; revised 22 Jun 2011; accepted 23 Jun 2011; published 14 Jul 2011

1.1. Mie Scattering

Mie scattering is valid for spheres of any size and is proportional to λ^{-b}. The exponent b varies with particle size, and has the value $b = 4$ for particles that are very small compared to the wavelength, in which case Mie scattering reduces to Rayleigh scattering. Recently, Jacques [30] showed that the value of b for skin epidermis and dermis tissues is equal to 0.838.

Using Mie theory, one can compute the light scattered by a homogeneous spherical particle at any point inside or outside the particle for a given size and refractive index relative to the host medium. For an observation distance from the center of the sphere that is large compared to the wavelength, the scattered field is given as a function of the *scattering angle* Θ, which is the angle between the directions of the incident and scattered radiation. Details of the Mie scattering theory are available elsewhere [31–33]. In the far zone, the electric field scattered by an arbitrarily shaped particle can be represented as an outgoing spherical wave whose complex amplitude and polarization is related to that of the incident electric field by a 2×2 matrix $S(\Theta)$ in the following form [31]

$$\begin{pmatrix} E_{\parallel s} \\ E_{\perp s} \end{pmatrix} = \frac{e^{ik(r-z)}}{-ikr} \begin{pmatrix} S_2 & S_3 \\ S_4 & S_1 \end{pmatrix} \begin{pmatrix} E_{\parallel i} \\ E_{\perp i} \end{pmatrix}. \tag{3}$$

Here the scattered electric-field components $E_{\parallel s}$ and $E_{\perp s}$ are considered at observation points sufficiently far ($kr \gg 1$) from the sphere so that the radial component of the scattered electric field becomes negligible. If the scattering particle is a homogeneous and isotropic sphere, then $S_3 = S_4 = 0$, so that the scattering matrix $S(\Theta)$ of such a sphere is given by

$$S(\Theta) = \begin{pmatrix} S_2(\Theta) & 0 \\ 0 & S_1(\Theta) \end{pmatrix}. \tag{4}$$

The scattering functions $S_1(\Theta)$ and $S_2(\Theta)$, which provide the perpendicular and parallel polarization components of the scattered electric field vector, are given by [31]

$$S_1(\Theta) = \sum_{n=1}^{\infty} \frac{2n+1}{n(n+1)} [a_n \pi_n(\mu) + b_n \tau_n(\mu)] \tag{5a}$$

$$S_2(\Theta) = \sum_{n=1}^{\infty} \frac{2n+1}{n(n+1)} [b_n \tau_n(\mu) + a_n \pi_n(\mu)] \tag{5b}$$

where n is a summation index and a_n and b_n are coefficients that depend on the size parameter x and the refractive index of the spherical particle relative to that of the host medium, which is assumed to be homogeneous, isotropic, and non-absorbing. The functions $\pi_n(\mu)$ and $\tau_n(\mu)$ with $\mu = \cos\Theta$ determine the angular dependence of the scattered field and are given in terms of associated Legendre polynomials [34].

Theoretically, the series expansions in terms of a_n and b_n in Eqs. (5a) and (5b) have an infinite number of terms, but in practical computations the summation must be terminated after a certain number of terms. According to Bohren and Huffman [31], the maximum number of terms required for convergence is given by $n = x + 4x^{1/3} + 2$.

When $\Theta = 0$, S_1 and S_2 become identical, indicating that scattering by spheres in the forward direction ($\Theta = 0$) is independent of the polarization state of the incident field. The total power extinction in the forward direction is given by [35]

$$Q_{ext} = \frac{4}{x^2} \Re\{S(\Theta = 0)\} \tag{6}$$

#146310 - $15.00 USD Received 28 Apr 2011; revised 22 Jun 2011; accepted 23 Jun 2011; published 14 Jul 2011

where Q_{ext} is the extinction efficiency and $\Re$ denotes the real part. As expected, Q_{ext} vanishes as $x \to 0$. Q_{ext} increases to 4 for $x \approx 1$, and deceases to 2 as the particle becomes very large ($x \to \infty$). Mie theory is generally applicable to scattering by homogeneous spheres of any size. For large values of x, the total extinction Q_{ext} tends to 2, implying that the extinction cross section becomes twice as large as the geometrical cross section, a result known as the extinction paradox [32].

The extinction efficiency Q_{ext} and scattering efficiency Q_{sca} of a spherical particle are given by [31, 32]

$$Q_{ext}(m,x) = \frac{2}{x^2}\sum_{n=1}^{\infty}(2n+1)\Re(a_n+b_n) \tag{7a}$$

$$Q_{sca}(m,x) = \frac{2}{x^2}\sum_{n=1}^{\infty}(2n+1)(|a_n|^2+|b_n|^2) \tag{7b}$$

where m is the relative refractive index of the particle. If the extinction does not involve absorption, the single-scattering albedo, which is the ratio of the scattering coefficient μ_s to the extinction coefficient $\mu_e = \mu_s + \mu_a$, is equal to unity. However, in skin tissue, the extinction generally includes absorption, so that the absorption efficiency Q_{abs} can be obtained from

$$Q_{abs}(m,x) = Q_{ext}(m,x) - Q_{sca}(m,x). \tag{8}$$

1.2. Scattering Phase Function

The angular distribution of the radiance associated with radiation scattered by a single particle is described by the scattering phase function, which depends on the scattering angle Θ. The scattering phase function can be normalized to unity [36], *i.e.*

$$\frac{1}{4\pi}\int_{4\pi} d\omega\, p(\mu) = \frac{1}{2}\int_{-1}^{1} d\mu\, p(\mu) = 1 \tag{9}$$

where $\cos\Theta = \mu$, and $d\omega$ is the differential solid angle centered around the direction of scattering. The scattering phase function $p(\mu)$ can be expanded in a series of Legendre polynomials such that

$$p(\tau,\mu) \approx \sum_{\ell=0}^{2N-1}(2\ell+1)\chi_\ell(\tau)P_\ell(\mu) \tag{10}$$

where τ is the optical depth and $\chi_\ell(\tau)$ is ℓth expansion coefficient given by

$$\chi_\ell(\tau) = \frac{1}{2}\int_{-1}^{1} d\mu\, P_\ell(\mu)\, p(\tau,\mu), \tag{11}$$

and P_ℓ is the ℓth Legendre polynomial. The first expansion coefficient or moment χ_1 in Eq. (11) is called the *asymmetry factor g*, and is given by

$$g = \chi_1(\tau) = \frac{1}{2}\int_{-1}^{1} d\mu\, \mu\, p(\tau,\mu) \tag{12}$$

where g, which is confined to the range $-1 \le g \le +1$, is dimensionless and characterizes the direction of a single-scattering. For particles that are large relative to the wavelength of the incident radiation, the scattering phase function peaks towards the forward direction ($\Theta =$

#146310 - $15.00 USD Received 28 Apr 2011; revised 22 Jun 2011; accepted 23 Jun 2011; published 14 Jul 2011

0°), and then g tends to +1. When g tends to -1, the scattering is in the backward direction ($\Theta = 180^\circ$). If $g = 0$, the scattering is symmetric around $\Theta = \pi/2$. The asymmetry factor g for Rayleigh scattering is zero because the scattering phase function is proportional to $1 + \cos^2\Theta$, and hence is symmetric around $\Theta = \pi/2$. The parameters μ_a, μ_s, and g depend on the wavelength and the particle's size and relative refractive index.

The scattering phase function p, as given in Eqs. (9)-(10), is related to the total scattered intensity and is a function of the scattering angle Θ and the size parameter x as well as of the wavelength λ and applies to unpolarized radiation. For polarized light a 4×4 *phase matrix* is needed, and the phase function is the (1,1) element of the phase matrix. The asymmetry factor g in Eq. (12) with the scattering phase function $p(\mu)$ as given in Eq. (10) is valid for a single spherical particle, and can be analytically expressed in terms of the coefficients a_n and b_n without explicit knowledge of $p(\mu)$ [32]:

$$g = \frac{4}{x^2 Q_{sca}} \sum_{n=1}^{\infty} \frac{2n+1}{n(n+1)} \Re(a_n b_n^*) + \frac{4}{x^2 Q_{sca}} \sum_{n=1}^{\infty} \frac{n(n+2)}{n+1} \Re(a_n a_{n+1}^* + b_n b_{n+1}^*) \tag{13}$$

where the asterisk symbol denotes the complex conjugate.

1.3. Collection of Particles

Mie theory describes the extinction efficiency of a single homogeneous sphere. The extinction due to scattering by a collection of identical homogeneous spheres is simply the number of spheres times the scattering coefficient μ_s for a single particle, provided the scattering is independent. The human skin is an inhomogeneous, turbid optical medium in which the actual particle size distribution and refractive index vary with location. Such an inhomogeneous scattering medium can be decomposed into elementary volumes in each of which the particle distribution can be considered as homogenous [37] so that the extinction strength in each elementary volume is given by the product of the single particle extinction and the number of particles.

In order to average the scattering effects of a collection of inhomogeneous, poly-dispersed spheres, we represent the scattering particles by a log-normal size distribution [38] function $n(r)$ consisting of 20 evenly spaced size intervals dr within the range from $r_1 = \bar{r} - 3\sigma$ to $r_2 = \bar{r} + 3\sigma$ such that

$$n(r) = \frac{N}{r\sigma(2\pi)^{\frac{1}{2}}} \exp\left[-\frac{(\ln r - \bar{r})^2}{2\sigma^2}\right], \quad r > 0 \tag{14}$$

where $\bar{r}$ and σ are the mean and the standard deviation of the natural logarithm of the variable r. The number N which represents particles of all sizes in a unit volume is given by

$$\int_{r_1}^{r_2} n(r)dr = N. \tag{15}$$

The ensemble-averaged extinction coefficient $\tilde{\mu}_e(\lambda) = \tilde{\mu}_a(\lambda) + \tilde{\mu}_s(\lambda)$ and the ensemble-averaged scattering coefficient $\tilde{\mu}_s(\lambda)$ for a collection of spherical particles can be approximated as a weighted average of the contributions from individual particles as follows [39], *i.e.*

$$\tilde{\mu}_e(\lambda) = \pi \int_{r_1}^{r_2} r^2 Q_{ext}(m,x)\, n(r)\, dr \tag{16a}$$

$$\tilde{\mu}_s(\lambda) = \pi \int_{r_1}^{r_2} r^2 Q_{sca}(m,x)\, n(r)\, dr \tag{16b}$$

#146310 - $15.00 USD Received 28 Apr 2011; revised 22 Jun 2011; accepted 23 Jun 2011; published 14 Jul 2011

and the ensemble-averaged absorption coefficient for the collection then follows from $\tilde{\mu}_a(\lambda) = \tilde{\mu}_e(\lambda) - \tilde{\mu}_s(\lambda)$.

The ensemble-averaged asymmetry factor $\tilde{g}$ for a collection of particles is given by [23, 40]

$$\tilde{g}(\lambda) = \frac{1}{\tilde{\mu}_s(\lambda)} \int_{r_1}^{r_2} C_{sca}(m,r,\lambda)\, g(r,\lambda)\, n(r)\, dr \tag{17}$$

where $C_{sca} = \pi r^2 Q_{sca}$ is the scattering cross section of a particle with radius r.

The total ensemble-averaged scattering coefficient $\tilde{\mu}_s$ includes contributions due to Rayleigh scattering $\tilde{\mu}_s^R$ and Mie scattering $\tilde{\mu}_s^M$. We let $\tilde{\mu}_s^R$ be equal to $K\lambda^{-4}$, where the constant K represents the strength of Rayleigh scattering. With contributions from both types of scattering, the ensemble-averaged asymmetry factor $\tilde{g}$ becomes

$$\tilde{g}(\lambda) = \frac{\tilde{g}^R\, \tilde{\mu}_s^R + \tilde{g}^M\, \tilde{\mu}_s^M}{\tilde{\mu}_s^R + \tilde{\mu}_s^M} = \frac{\tilde{g}^M\, \tilde{\mu}_s^M}{\tilde{\mu}_s^R + \tilde{\mu}_s^M} \tag{18}$$

where the last result follows from the fact that $\tilde{g}^R = 0$, since, as mentioned previously, the Rayleigh scattering phase function is symmetric around $\Theta = \pi/2$.

2. Method

2.1. Bio-optical Model

Bio-optical models (BOMs) are generally used in conjunction with radiative transfer in aquatic media [39, 44]. In that case, a BOM provides a link between IOPs (absorption coefficient, scattering coefficient, and asymmetry factor) and water constituents (such as concentrations of chl-*a*, colored dissolved organic matter (CDOM), and suspended matter). However, BOMs that describe the optics of living tissue, such as human skin tissue, are rarely found in the open literature. A simple BOM for human skin was presented by Nielsen et al. [4], who generated IOPs (μ_a, μ_s, and g) for melanosome particles from Mie theory in the UV spectral region (250–310 nm). They considered the real part of the refractive index of the melanosome particles to be constant, whereas the refractive index of human skin is actually wavelength dependent [22, 45] in the VIS and NIR spectral ranges.

We used a BOM developed by Balter Medical AS that was developed for non-invasive

Table 1. Input parameters to Balter BOM.

Layer	$dz\,[mm]$	volume fraction [%]	Types of particles
Upper Epidermis	0.02	40	melanosomes (10%), keratin (30%)
Lower Epidermis	0.08	40	melanosomes (10%), keratin (30%)
Dermis	1.00	HbO (75%) and Hb (2%)	blood, collagen
Sub-cutis	3.00	60	fat, intralipid

monitoring of skin tissue using backscattered light [4, 46]. This Balter BOM generates IOPs (optical thickness τ_B, single-scattering albedo ω_B, and scattering phase function asymmetry factor g_B) for each layer of the skin from layer thickness and particle concentrations or particle volume fractions. The Balter BOM is also based on additional inputs from the literature, such as fat absorption coefficient [47], water absorption coefficient [48], and blood absorption coefficient [49].

In the Balter BOM, the skin is divided in the following four layers of different thickness: *upper epidermis, lower epidermis, dermis*, and *sub-cutis*. For each of these four layers, the layer

#146310 - $15.00 USD Received 28 Apr 2011; revised 22 Jun 2011; accepted 23 Jun 2011; published 14 Jul 2011

thickness dz, the volume fraction of particles [%], and the major types of particles used as input to the Balter BOM are summarized in Table 1.

For a skin layer with thickness dz, the Balter BOM generates the differential optical thickness $d\tau_B(\lambda)$, the single-scattering albedo $\omega_B(\lambda)$, and the asymmetry factor $g_B(\lambda)$, which can be expressed in terms of the ensemble-averaged absorption coefficient $\tilde{\mu}_a(\lambda)$, scattering coefficient $\tilde{\mu}_s(\lambda)$, and asymmetry factor $\tilde{g}^M$ for Mie scattering derived in section 1.2, *i.e.*

$$\mu_{e,B}(\lambda) = \frac{d\tau_B(\lambda)}{dz} = \tilde{\mu}_a(\lambda) + \tilde{\mu}_s(\lambda) = \tilde{\mu}_e(\lambda) \tag{19}$$

$$\mu_{s,B}(\lambda) = \omega_B(\lambda)\,\frac{d\tau_B(\lambda)}{dz} = \tilde{\mu}_s(\lambda) \tag{20}$$

$$\mu_{a,B}(\lambda) = [1-\omega_B(\lambda)]\,\frac{d\tau_B(\lambda)}{dz} = \tilde{\mu}_a(\lambda) \tag{21}$$

$$g_B = \frac{\tilde{g}^M \tilde{\mu}_s^M}{\tilde{\mu}_s^M + \tilde{\mu}_s^M}. \tag{22}$$

For each layer, we compared the BOM-generated quantity on the left side of Eqs. (19), (20), and (21) with respectively $\tilde{\mu}_e(\lambda)$, $\tilde{\mu}_s(\lambda)$, and $\tilde{\mu}_a(\lambda)$ on the right side obtained from Rayleigh and Mie scattering theory. Similarly, for each layer, we compared the BOM-generated asymmetry factor g_B on the left side of Eq. (22) with the quantity on the right side obtained from Rayleigh and Mie scattering theory. These comparisons were performed using least-squares fitting in MATLAB^{TM} by varying the complex refractive index and the size distribution of the particles until satisfactory agreement was obtained between the BOM-generated IOPs and those obtained from Rayleigh and Mie scattering theory.

2.2. Least-squares Fitting

We implemented the Nelder-Mead simplex method in the MATLAB function *fminsearch* to match the BOM-generated IOPs with those obtained from Rayleigh and Mie scattering theory. This direct search method [50] has been widely used for the optimization of simulation models since its publication [51] in 1965. For a multidimensional objective function of n real variables, each iteration in this algorithm includes the evaluation of the objective function at each of a set of $n+1$ points or *vertices* in n dimensional space (*simplex*) through reflection, expansion, and contraction [52]. The iteration starts with initial guess values of the variables and continues until specified stopping criteria are reached.

Our objective function, which gives the absolute difference between the BOM-generated quantities $\mu_{a,B}(\lambda)$, $\mu_{s,B}(\lambda)$, and $g_B(\lambda)$ and the corresponding quantities $\tilde{\mu}_a(\lambda)$, $\tilde{\mu}_s(\lambda)$, and $\tilde{g}(\lambda)$ obtained from Rayleigh and Mie scattering theory, is given by

$$f(m,x) = \frac{1}{10}\left\{\sum_{j=1}^{10}\left[\left(1-\frac{\tilde{\mu}_a(\lambda_j)}{\mu_{a,B}(\lambda_j)}\right)^2 + \left(1-\frac{\tilde{\mu}_s(\lambda_j)}{\mu_{s,B}(\lambda_j)}\right)^2 + \left(1-\frac{\tilde{g}(\lambda_j)}{g_B(\lambda_j)}\right)^2\right]^{\frac{1}{2}}\right\} \tag{23}$$

where $f(m,x)$ is the sum of the *least-squares* differences between the IOPs at ten different wavelengths. These ten wavelengths, which are unevenly distributed in the range from the near UV to the NIR, are used in measurements performed with a skin scanner designed and built by Balter Medical AS, Norway [53].

The starting values used to initialize the objective function in Eq. (23) were a set of real-valued variables represented by m', m'', $\bar{r}$, σ, and K, where $m = m' + im''$ is the complex refractive index of the particles, $\bar{r}$ and σ are the mean and the standard deviation of the particle

#146310 - $15.00 USD Received 28 Apr 2011; revised 22 Jun 2011; accepted 23 Jun 2011; published 14 Jul 2011

size distribution, and K is the strength of the Rayleigh scattering. In the simulations, $\tilde{\mu}_a(\lambda)$ was sensitive to the imaginary part m'' of the refractive index, whereas $\tilde{\mu}_s(\lambda)$ and the $\tilde{g}(\lambda)$ were sensitive to the real part m' of the refractive index as well as to $\bar{r}$ and σ. The parameters $\tilde{\mu}_a(\lambda_j)$, $\tilde{\mu}_s(\lambda_j)$, and $\tilde{g}(\lambda_j)$ appearing in our objective function Eq. (23) were obtained from computer programs published by Bohren and Huffmann [31, appendix A], which were implemented in MATLAB functions by M*ä*tzler [54].

3. Results and Discussion

Human skin is a heterogeneous optical medium containing particles of various sizes, shapes and refractive indices at different depths. Thus, light incident on the air-skin interface will be partly reflected and partly transmitted, and the transmitted part will be absorbed and scattered inside the tissue depending on its IOPs.

To describe light transport in skin, one may model the tissue as plane-parallel layers of finite thickness with given IOPs (absorption coefficient, scattering coefficient, and scattering phase function), based on the assumption of no variation in the IOPs in directions parallel to the layers. Then, for a light beam incident in a given direction upon the air-skin interface, the directional light distribution at a given depth beneath the skin surface as well as the light emerging from the skin in a given direction can be obtained by solving the radiative transfer equation for a coupled air-tissue system [55]. Also, the light emerging from the skin in a specified direction can be measured, and such measurements can be used to retrieve skin physiological parameters [41], which are related to corresponding IOPs by a bio-optical model [see Eqs. (19) - (22)]. Since the IOPs of human skin vary with depth, we use a multi-layered plane-parallel model with layer-dependent IOPs.

Using a seven-layer skin model comprised of five epidermal layers, one dermis layer, and one sub-cutis layer, Nielsen et al. [4] simulated wavelength-dependent reflectance spectra and asymmetry factors due to melanosome particles in the spectral range from 250 to 700 nm. They showed that strongly pigmented skin absorbs less UV radiation than weakly pigmented skin in the spectral range $250 \leq \lambda \leq 300$ nm. Magnain et al. [56] used a 22-layer model of human skin to show that the variation of the reflectance characteristics in the VIS spectral region depends on particle concentrations and layer thickness. In the simulations, they varied the concentrations of melanin and keratin in the epidermis and collagen and hemoglobin in the dermis, and they compared simulated results with measured reflectance spectra for different skin colors.

Light transport in a complex skin structure is strongly affected by particle size distributions and shapes as well as by the particle number density and the wavelength dependent, complex refractive index. These properties vary between different layers, making the penetration of light into different skin layers dependent on wavelength. We considered a model of human skin consisting of four layers: upper epidermis, lower epidermis, dermis, and sub-cutis with thickness dz as given in Table 1, and assumed spherical particles to be present in each layer with a complex refractive index value to be determined at each of ten different wavelengths in the VIS and NIR spectral ranges. In each layer, the particle size distribution and complex refractive index were determined at each of the ten wavelengths by fitting the modeled and calculated spectral values of the absorption coefficient μ_a, the scattering coefficient μ_s (Mie + Rayleigh), and the asymmetry factor g. The Rayleigh scattering coefficient was assumed to be the same in each layer, given by $\mu_{s,Ray} = K(\lambda)\,\lambda^{-4}$, where the strength factor K was allowed to vary with λ. Because of the λ^{-4} dependence, Rayleigh scattering decreases rapidly as the wavelength increases.

3.1. Stratum Corneum or Upper epidermis

As mentioned above, Nielsen et al. [4] used a seven-layer skin model comprised of five epidermal layers, one dermis layer, and one sub-cutis layer. In the Balter BOM, the uppermost of the

#146310 - $15.00 USD Received 28 Apr 2011; revised 22 Jun 2011; accepted 23 Jun 2011; published 14 Jul 2011

five epidermal sub-layers is called the *upper epidermis*, which is assumed to represent the stratum corneum. It is the outermost layer of the skin that protects the underlying skin tissue from the external environment. The upper epidermis layer consists of nonviable or dead keratinocyte cells mixed with melanin dust. Thus, we considered most particles in the upper epidermis layer to consist of keratin and melanin, whose volume fractions and layer thickness used as input to the Balter BOM are given in the Table 1. In the upper epidermis, part of the scattering takes place at the air-tissue surface, whereas in the subsurface layers scattering is due only to particles that are embedded in the host medium. In this respect, the scattering process in the upper epidermis can be distinguished from that in an underlying layer.

Figure 1 shows the log-normal size distribution and IOPs of the upper epidermis, where par-

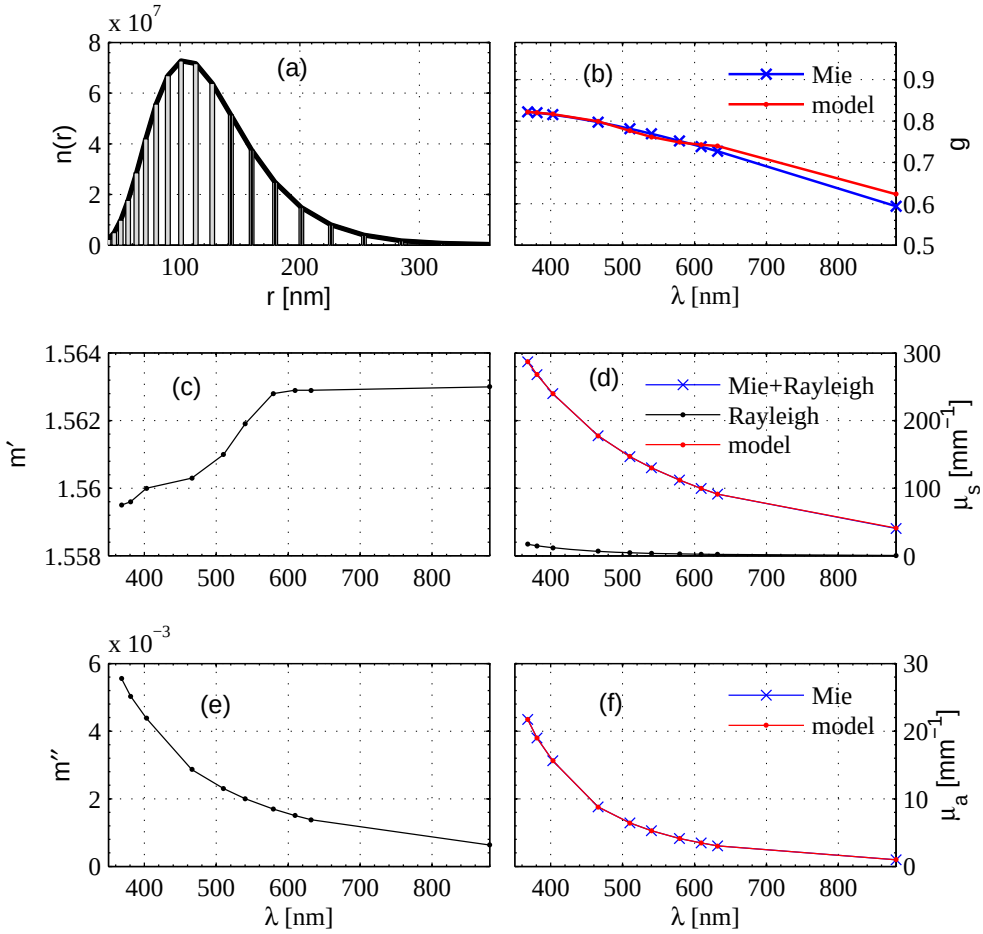

Fig. 1. Optimized IOPs in the upper part of the epidermis. (a) Log-normal particle size distribution $n(r)$ [(mm)$^{-3}$(nm)$^{-1}$]. (b) Asymmetry factor g. (c) Real part m' of the refractive index. (d) Scattering coefficient μ_s. (e) Imaginary part m'' of the refractive index. (d) Absorption coefficient μ_a.

ticle radii vary from 40 to 360 nm with a log-normal mean radius of $\bar{r} = 128$ nm. The absorption coefficient μ_a, the scattering coefficient μ_s, and the imaginary part m'' of the refractive index were found to decrease with increasing λ [cf. Figs. 1(d)–(f)], whereas the real part m' of the

#146310 - $15.00 USD Received 28 Apr 2011; revised 22 Jun 2011; accepted 23 Jun 2011; published 14 Jul 2011

refractive index was found to increase slightly [cf. Fig. 1 (c)]. Since the variation in the absolute value of m' between $\lambda = 368$ nm and $\lambda = 880$ nm is fairly small (0.19%), it is considered to have the constant value of $m' \simeq 1.56$ in this layer. The melanosomes are assumed to become smaller due to fragmentation as they are transported upwards from the lower epidermis and to end up as melanin dust in the upper epidermis. The melanin dust both absorbs and scatters light, whereas keratin is assumed to act only as an absorber. We considered these particles to be mixed in a host or base medium with real part of the refractive index of $m' = 1.36$. Thus, in the upper epidermis there are two types of particles, which scatter light in accordance with Mie and Rayleigh scattering theory. Rayleigh scattering, which contributes only about 6% to the total scattering at $\lambda = 368$ nm, decreases with increasing λ and contributes less than 1% at $\lambda = 880$ nm. The asymmetry factor g depends on the size distribution of the scattering particles. The value of g obtained from Mie computations was found to agree well with that provided by the Balter BOM for wavelengths in the range from $\lambda = 368$ nm to $\lambda = 632$ nm. However at $\lambda = 880$ nm, the value of g was found to be 4% lower than that obtained from the Balter BOM.

3.2. Lower epidermis

As mentioned above, in the Balter BOM, the outermost layer of the five epidermis sub-layers of Nielsen et al. [4] is called the *upper epidermis*. The remaining five sub-layers constitute the *lower epidermis* which is assumed to have a thickness equal to four times that of the upper epidermis. The lower epidermis is a bloodless layer, in which the most common cells are keratinocytes, melanocytes, and langerhans. These cells are immersed into the base fluid, which is slightly more dense than water. As in the upper epidermis, keratin in the lower epidermis is considered to only absorb light, whereas melanin is considered both to absorb and scatter light. Similarly to scattering in the upper epidermis, scattering in the lower epidermis depends on the amount of melanin in the base medium, whereas the absorption is determined by the amounts of both keratin and melanin.

The particle size distribution with radii varying from 50 to 740 nm is shown in Fig. 2(a), and the log-normal mean radius $\bar{r}$ is equal to 206 nm which is found to be 1.6 times larger than that in the upper epidermis. This result is consistent with the prediction that the size of melanosome particles decreases as they move upward from the lower epidermis to the upper epidermis [19]. In the lower epidermis, the absolute value of m' varies smoothly by 0.39% when the wavelength varies from $\lambda = 368$ nm to $\lambda = 880$ nm, which is twice as large as the corresponding variation in the upper epidermis. This trend is opposite to that found in published results [22, 57]. However, since the variation with wavelength of m' in the lower epidermis is fairly small, we may regard it to have a constant value, i.e., $m' \simeq 1.52$ for wavelengths in the range $\lambda = 368 - 880$ nm.

The variation of the IOPs in the lower epidermis (Fig. 2) is similar to that in the upper epidermis (Fig. 1). However, the asymmetry factor g and the scattering coefficient μ_s in the lower epidermis are found to be larger than those in the upper epidermis, while absorption and Rayleigh scattering coefficients are seen to be the same in both epidermis layers. The contribution from Rayleigh scattering to the total scattering is 4% at $\lambda = 368$ nm, and decreases with increasing λ to less than 1% at $\lambda = 880$ nm.

3.3. Dermis

In the dermis layer of human skin, light is absorbed and scattered by collagen, hemoglobin, plasma fluids, and other substances, such as fat and water particles. In this layer, the log-normal distribution of particle radii are found to vary from 80 nm to 1.8 μm with log-normal mean radius of $\bar{r} = 449$ nm. The particle size distribution, refractive-index variation with wavelength,

#146310 - $15.00 USD Received 28 Apr 2011; revised 22 Jun 2011; accepted 23 Jun 2011; published 14 Jul 2011

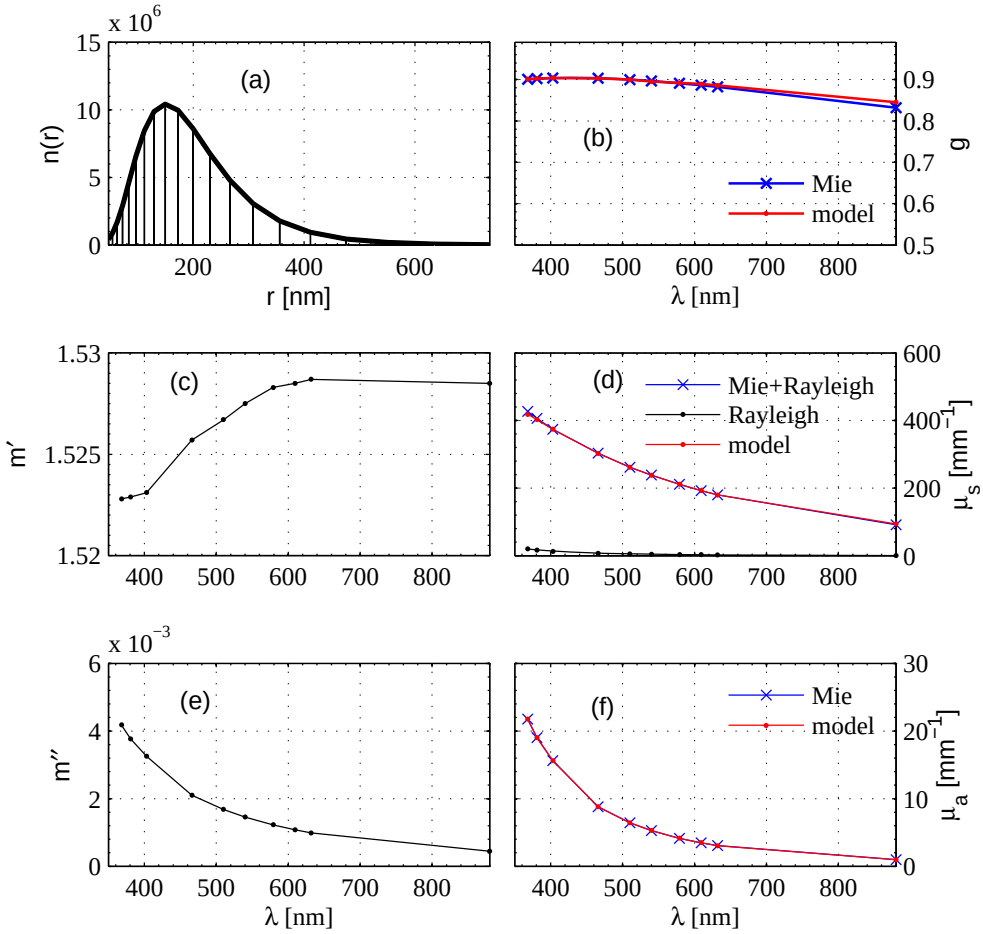

Fig. 2. Optimized IOPs in the lower epidermis. (a) Log-normal particle size distribution $n(r)$ [(mm)$^{-3}$(nm)$^{-1}$]. (b) Asymmetry factor g. (c) Real part m' of the refractive index. (d) Scattering coefficient μ_s. (e) Imaginary part m'' of the refractive index. (f) Absorption coefficient μ_a.

and associated IOPs of the dermis, obtained from the optimization, are given in Fig. 3. In the VIS spectral region, the wavelength-dependent absorption in the dermis is due to *de-oxygenated* (Hb) and *oxygenated* (HbO_2) hemoglobin. Fig. 3(f) shows the dermis absorption coefficient μ_a, which has peak values at 403 and 540 nm. At these wavelengths, the imaginary part m'' of the refractive index also has peak values [cf. Figs 3 (e)-(f)]. But both m'' and μ_a are seen to have very low values at wavelengths above 600 nm.

Figure 3(d) shows that the scattering coefficient μ_s of the dermis layer decreases with increasing λ. The contribution from Rayleigh scattering to the total scattering coefficient is less than 5% at $\lambda = 880$ nm, but increases to 40% at $\lambda = 368$ nm. Scattering by hemoglobin in the VIS and NIR spectral regions was discussed by Faber et al. [6], who showed that Hb particles scatter 10% less than HbO_2 particles at $\lambda > 600$ nm, but that HbO_2 particles scatter slightly more than Hb particles at $\lambda < 400$ nm. Besides scattering by hemoglobin, dermis scattering is due primarily to collagen particles, whose sizes vary from micrometer [45] to nanometer in

#146310 - $15.00 USD Received 28 Apr 2011; revised 22 Jun 2011; accepted 23 Jun 2011; published 14 Jul 2011

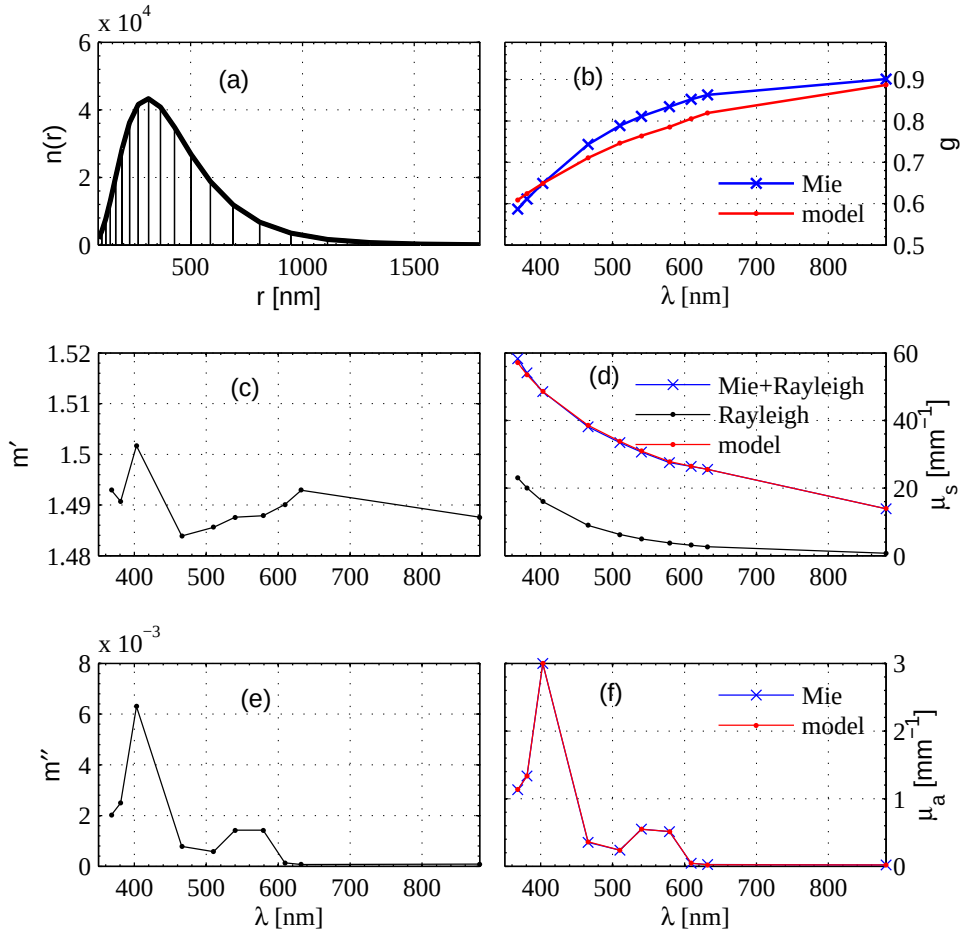

Fig. 3. Optimized IOPs in the dermis. (a) Log-normal particle size distribution $n(r)$ [(mm)$^{-3}$(nm)$^{-1}$]. (b) Asymmetry factor g. (c) Real part m' of the refractive index. (d) Scattering coefficient μ_s. (e) Imaginary part m'' of the refractive index. (f) Absorption coefficient μ_a.

diameter.

Figure 3(b) shows that the asymmetry factor g obtained from the Balter BOM is somewhat different from that obtained from Mie calculations, in contrast to the corresponding results for the epidermis layers (Figs. 1-2) and the sub-cutis layer (Fig. 4). This difference is present both below and above $\lambda = 403$ nm, where the absorption has its maximum value [cf. Fig. 3(f)], and the maximum difference is at $\lambda = 623$ nm. The difference between the asymmetry factors obtained from the Balter BOM and Mie calculations is larger (5%) in the dermis than in the other skin layers, which may be related to the larger variation of particle sizes in the dermis and its possible absorbing nature. A large amount of small particles contributes to the strength of Rayleigh scattering and affects the averaged asymmetry factor. Also, if the host medium is absorbing, it influences the scattering phase function for the larger size particles [24].

#146310 - $15.00 USD Received 28 Apr 2011; revised 22 Jun 2011; accepted 23 Jun 2011; published 14 Jul 2011

3.4. *Sub-cutis*

The sub-cutis layer consists of fat cells, nerves, and blood vessels. It is the lower-most layer of the skin with a typical thickness of 3 mm, and has almost no absorption [47] in the VIS spectral region. As shown in Fig. 4(a), the distribution of particle radii vary from 130 to 250 nm, with a mean particle radius of $\bar{r} = 182$ nm, which is larger than that in the upper epidermis, but smaller than that in the lower epidermis or in the dermis. The IOPs are shown in Fig. 4(b), (d), and (f). The contribution from Rayleigh scattering to the total scattering is less than 1% within the entire range of wavelengths. Thus, in the sub-cutis layer, Mie scattering by particles having size parameters in the range $1.3 \leq x \leq 5.7$ dominates. In this layer, the absorption coefficient μ_a,

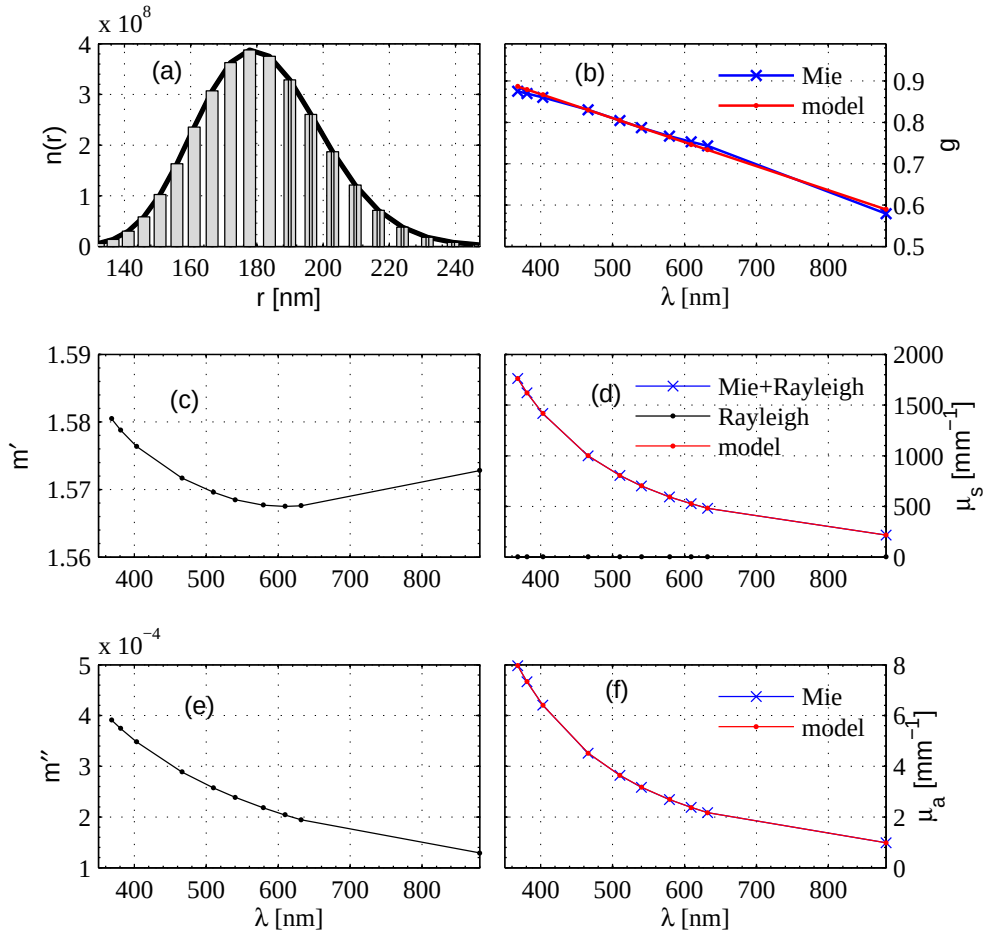

Fig. 4. Optimized optical properties in Sub-cutis: (a) log-normal distribution $n(r)$ [(mm)$^{-3}$ (nm)$^{-1}$] of particles size, (b) Asymmetry factor g, (c) real part of refractive index m', (d) the scattering coefficient μ_s, (e) imaginary part of refractive index m'', and (f) absorption coefficient μ_a.

the scattering coefficient μ_s, and the asymmetry factor g are found to decrease with increasing wavelength, and the scattering coefficient μ_s is larger than in any other layer. The imaginary part m'' of the refractive index is seen to decrease with increasing wavelength, whereas the real

#146310 - $15.00 USD Received 28 Apr 2011; revised 22 Jun 2011; accepted 23 Jun 2011; published 14 Jul 2011

part m' stays fairly constant with an average value of 1.57 for wavelengths above 500 nm. At wavelengths below 500 nm, m'' [Fig. 4(e)], the absorption coefficient [Fig. 4(f)], m' [Fig. 4(c)] and the scattering coefficient [Fig. 4(d)], all have relatively high values. Therefore, the sub cutis layer is opaque to incident light at wavelengths below 500 nm.

3.5. Discussion

The size range of spherical particles used in the Mie computations is shown in Figs. 1–4(a) for the four skin layers. The mean radius $\bar{r}$ and the variance v for each layer are given in Table 2, which shows that the mean particle diameter varies from 256 nm in the upper epidermis to 898 nm in the dermis. The larger particles, which are about 3.5 μm in diameter, are most probably non-oxygenated and oxygenated hemoglobin particles and collagen fibers in the dermis layer. In the dermis, the cellular structures of small-scaled collagen fibers have sizes in the range from 60 to 100 nm [8], whereas collagen bundles and hemoglobin particles have sizes in the order of a few μm. Other particles contained in the dermis may originate from fat and water with sizes smaller than those of collagen and blood particles. The smallest particles with diameters of about 80 nm, which are found in the upper epidermis, may be melanosome dust produced by the fragmentation of melanin. The diameters of melanosome particles [3, 4] range from 100 to 1,000 nm, and the largest melanosome particles are found in the lower epidermis.

The optimized values for the complex refractive index $m = m' + i\,m''$ in the four different skin layers are shown in Table 2 for different wavelengths, and these results are plotted in Figs. 1–4(c) for the real part m' and in Figs. 1–4(e) for the imaginary part m''. The highest value of m' is found in the sub-cutis layer, and the lowest value in the dermis. The opposite is true for the imaginary part m'' of the refractive index, *i.e.* m'' has its lowest values in the sub-cutis and its highest values in the dermis. Therefore, the dermis is the most light-absorbing layer, whereas the sub-cutis is the most light-scattering layer. Both m' and m'' are slightly higher in the upper epidermis layer than in the lower epidermis layer. The refractive-index values in the four skin layers are such that $m'_{sc} > m'_{ue} > m'_{le} > m'_{de}$, whereas $m''_{de} > m''_{le} = m''_{ue} > m''_{sc}$, where the subscripts *sc*, *de*, *le*, and *ue*, stand for sub-cutis, dermis, lower epidermis, and upper epidermis, respectively. Note that the lower epidermis is four times thicker than the upper epidermis in the Balter BOM.

We expected our optimized refractive-index values to compare reasonably well with those published for biological tissues. Tuchin et al. [58] showed that for collagen fibers $m' = 1.474$ at $\lambda = 589$ nm. In our result, m' = 1.488 at $\lambda = 579$ nm for the dermis, where the scattering is most likely dominated by collagen particles. Ding et al. [22] measured the complex refractive index m for Caucasian abdomen skin and found its real part to be higher for the epidermis than for the dermis. The data published by Ding et al. [22] cover a wider spectral range as ours. However, their m' values are lower than ours both for the epidermis and the dermis, and the difference is not the same at each wavelength. The complex refractive index for *in vitro* porcine tissues, including that of dermis tissues, was recently reported by Lai et al. [59], who found $m = 1.3818 + i0.0049$ at 632.8 nm for the dermis. This result for the real part of the refractive index is comparable to that found by Ding et al. [22] at the same wavelength, but the imaginary part found by Lai et al. [59] is higher than that found by Ding et al. [22].

Comparisons with results published in the open literatures [22, 45, 48, 58, 59] show that our size distributions and refractive indices are acceptable within the uncertainty quantified by the cost function $f(m,x)$ in Eq. (23). For the input parameters to the BOM in Table 1, the sum of the least square differences $f(m,x)$ between the BOM-generated IOPs and corresponding IOPs obtained from Rayleigh and Mie scattering theory is found to be different for the four skin layers such that $f(m,x)$ equals to 0.013 in the upper epidermis, 0.007 in the lower epidermis, 0.043 in the dermis, and 0.0074 in the sub-cutis. Refractive-index data accessible in the literature usually

#146310 - $15.00 USD Received 28 Apr 2011; revised 22 Jun 2011; accepted 23 Jun 2011; published 14 Jul 2011

do not cover a wide range of wavelengths. Moreover, available refractive-index data are mostly for the real part only, whereas a complete description of light transport in a medium such as skin tissue, requires knowledge of the complex refractive index for a wide range of different wavelengths, such as shown in Table 2.

The absorption is determined by the imaginary part m'' of the refractive index, while the

Table 2. Retrieved IOPs in human skin layers. The symbols $\bar{r}$ and v denote the log-normal mean radius and the variance, respectively, of the retrieved particle size distribution.

–	U. Epidermis	L. Epidermis	Dermis	Sub-cutis
–	$\bar{r} = 128$ nm	$\bar{r} = 206$ nm	$\bar{r} = 449$ nm	$\bar{r} = 182$ nm
–	$v = 2.3473 \times 10^3$	$v = 9.9493 \times 10^3$	$v = 5.8247 \times 10^4$	$v = 3.6209 \times 10^2$
$\lambda_0\,[nm]$	$m' + m'' \times 10^{-3}$	$m' + m'' \times 10^{-3}$	$m' + m'' \times 10^{-3}$	$m' + m'' \times 10^{-3}$
368	1.559+i5.561	1.523+i4.177	1.493+i2.021	1.580+i0.3915
381	1.560+i5.031	1.523+i3.764	1.491+i2.500	1.579+i0.3743
403	1.560+i4.374	1.523+i3.253	1.502+i6.297	1.576+i0.3483
466	1.560+i2.865	1.526+i2.103	1.484+i0.783	1.572+i0.2889
510	1.561+i2.303	1.527+i1.680	1.486+i0.579	1.570+i0.2574
540	1.562+i2.006	1.527+i1.456	1.488+i1.428	1.568+i0.2390
579	1.562+i1.698	1.528+i1.227	1.490+i1.427	1.568+i0.2181
609	1.562+i1.506	1.528+i1.083	1.490+i0.133	1.567+i0.2042
632	1.562+i1.377	1.529+i0.990	1.493+i0.074	1.567+i0.1945
880	1.562+i0.633	1.529+i0.445	1.488+i0.084	1.573+i0.1292

real part m' determines the scattering, which occurs due to the mismatch between the refractive index of the scattering particles and that of the host medium. Also, the mismatch of the refractive index at the air-skin interface causes a part of the incident light to be reflected. At normal incidence, the reflected light intensity will be $\simeq$5% of the incident light intensity if $m' = 1.56$ (see Table 2 for the upper epidermis). The portion of the light that penetrates into the skin tissue will be absorbed and scattered depending on the IOPs of the skin tissue. The variation in the IOPs between different body sites of a given individual is larger than the variation in the IOPs of a given body site between different individuals [7].

Since the values of μ_a and μ_s vary strongly with the amount of chromophores (due to skin pigments and blood content), modeled and measured IOPs can be matched by changing the values of these physiological parameters in the BOM that produces input to the radiative transfer simulations. Here it should be noted that the tabulated data used in the Balter BOM are measured, wavelength-dependent IOPs [4, 47–49]. For a review of experimental data, see the recent publication [57]. The light field in the volume below the skin surface is generally diffuse due to multiple scattering in random directions. However, the scattered light emerging from the surface is the sum of light reflected from the air-tissue interface and backscattered from beneath the skin surface, which in part is due to multiple scattering. The scattering asymmetry factor g, which is the average of the cosine of the scattering angle, is found to be different for different skin layers. According to Gemert et al. [11], the empirical value for g in the epidermis can be

#146310 - $15.00 USD Received 28 Apr 2011; revised 22 Jun 2011; accepted 23 Jun 2011; published 14 Jul 2011

considered nearly identical to that in the dermis, *i.e.*

$$g_{ep} \sim g_{de} \sim 0.62 + 0.29 \times 10^{-3}\ \lambda \tag{24}$$

where λ is in nm. The values of g calculated from Eq. (24) varies from 0.73 to 0.87 when λ varies from 368 to 880 nm. For the same range of wavelengths, the values of g from our optimizations vary from 0.82 to 0.59 in the upper epidermis, from 0.9 to 0.83 in the lower epidermis, from 0.59 to 0.90 in the dermis, and from 0.88 to 0.59 in the sub-cutis. These g values indicate that light scattering from skin layers always is peaked in the forward direction. According to Eq. (18), the size-averaged asymmetry factor $\tilde{g}$ depends on the strengths of both Rayleigh scattering and Mie scattering. As stated previously, the averaged g for Rayleigh scattering is zero. Therefore, the size-averaged asymmetry factor will be reduced when the strength of Rayleigh scattering increases, as seen in panels (b) and (d) of Fig. 3 for the dermis layer.

4. Conclusions

Light transport in a random medium like human skin can be described by the radiative transfer equation [60], which depends on IOPs, *i.e.* absorption coefficients, scattering coefficients, and scattering phase functions, as input. Since there is an abrupt change in the refractive across the air-tissue interface, solutions to the radiative transfer equation must take this change into account [36, 55]. We have described a novel method to determine the size distribution as well the complex refractive index of particles in several skin layers that can be used to compute the IOPs of skin required as input to radiative transfer models used to quantify the transport of unpolarized as well as polarized light inside the tissue and reflected from it. We have assumed human skin to be a non-absorbing host medium, consisting of four different layers with embedded ensembles of absorbing and scattering particles. We have assumed each skin layer to contain an ensemble of homogeneous spherical particles, and used Mie theory to compute the asymmetry factor of the scattering phase function as well as the absorption and scattering coefficients for a specified particle size distribution and specified values of the complex refractive index at various wavelengths. Using an optimization scheme, we have determined that particle size distribution and those complex refractive-index values for the particles as a function of wavelength in each of the four skin layers which provide best agreement between our optimized IOPs and those given by an existing bio-optical model.

The size distributions and the complex refractive indices tabulated in this paper, can be used to compute IOPs required as input to solve light transport problems in coupled air-skin tissue systems [41, 55]. Also, they can be used to compute the scattering phase matrix, which is an essential input to model polarized light transport in human skin tissue.

Applications of such IOPs may have extensive use in diagnostic, therapeutic, and cosmetic techniques in dermatology. For example, skin optics has special relevance to how light can be utilized in skin cancer diagnosis [43, 46] and photodynamic therapy [61].

Acknowledgement

This work was supported by the Research Council of Norway. We are grateful to Balter Medical AS for providing the bio-optical model and thankful to two anonymous reviewers for valuable comments and suggestions.

#146310 - $15.00 USD Received 28 Apr 2011; revised 22 Jun 2011; accepted 23 Jun 2011; published 14 Jul 2011